Full Text View

Volume 32, Issue 11 (November 2002)

Journal of Physical Oceanography
Article: pp. 3003–3019 | Abstract | PDF (579K)

Structure and Flow-Induced Variability of the Subtidal Salinity Field in Northern San Francisco Bay

Stephen G. Monismith

Environmental Fluid Mechanics Laboratory, Stanford University, Stanford, California

Wim Kimmerer

Romberg Tiburon Center, San Francisco State University, Tiburon, California

Jon R. Burau

Water Resources Division, California District, U.S. Geological Survey, Sacramento, California

Mark T. Stacey

Department of Civil and Environmental Engineering, University of California, Berkeley, Berkeley, California

(Manuscript received October 2, 2001, in final form March 14, 2002)

DOI: 10.1175/1520-0485(2002)032<3003:SAFIVO>2.0.CO;2

ABSTRACT

The structure of the salinity field in northern San Francisco Bay and how it is affected by freshwater flow are discussed. Two datasets are examined: the first is 23 years of daily salinity data taken by the U.S. Bureau of Reclamation along the axis of northern San Francisco Bay; the second is a set of salinity transects taken by the U.S. Geological Survey between 1988 and 1993. Central to this paper is a measure of salinity intrusion, X_2: the distance from the Golden Gate Bridge to where the bottom salinity is 2 psu. Using X_2 to scale distance, the authors find that for most flow conditions, the mean salinity distribution of the estuary is nearly self-similar with a salinity gradient in the center 70% of the region between the Golden Gate and X_2 that is proportional to X^{-1}_2. Analysis of covariability of Q and X_2 showed a characteristic timescale of adjustment of the salinity field of approximately 2 weeks. The steady-state response deduced from the X_2 time series implies that X_2 is proportional to riverflow to the 1/7 power. This relation, which differs from the standard 1/3

power dependence that is derived theoretically assuming constant exchange coefficients, shows that the upstream salt flux associated with gravitational circulation is more sensitive to the longitudinal salinity gradient than theory supposes. This is attributed to the strengthening of stratification caused by the stronger longitudinal salinity gradient that accompanies larger river flows.

1. Introduction

As a part of attempts to manage and restore the San Francisco Estuary, environmental standards have been based on the positioning of the salt field in northern San Francisco Bay and the adjoining delta of the Sacramento and San Joaquin Rivers (see Fig. 1). Following a suggestion by Williams and Hollibaugh (1989), the measure of salinity intrusion proposed by the Environmental Protection Agency (EPA; Schubel et al. 1992), and eventually implemented, was X_2—the distance (km) from the Golden Gate Bridge, measured along the main shipping channel, to the point where the salinity on the bottom is 2 psu. Analysis of time series of biological resources (fish and invertebrates) reported in Jassby et al. (1995) identified strong linkages between X_2 and abundance at all trophic levels. As part of that work, a quarter century of salinity data taken by the U.S. Bureau of Reclamation (USBR) was used to determine X_2 as a function of time and freshwater flow. This dataset permits us to take a rather comprehensive view of the way salinity intrusion, that is, X_2, depends on flow.

The dependence of salinity on flow and tidal conditions is fundamental to estuarine physics; accordingly, the dynamics of the salt balance that maintains that structure occupies a substantial part of the estuarine hydrodynamics literature. Put simply, river flow tends to carry salt out of the estuary, thus freshening it, whereas dispersion associated with tidal motions and baroclinic exchange flows, often represented by a Fickian diffusion coefficient, K_x, tend to transport salt downgradient and hence upstream into the river (Hansen and Rattray 1965; Fischer et al. 1979; Zimmerman 1986; Geyer et al. 2000; Bowen 2000; MacCready 1999). At steady state, these two processes are in balance whereas, when flows or tides change, the net salt flux can be either upstream or downstream. For reference purposes, this balance is embodied in the cross-sectionally and tidally averaged salt conservation equation:

$$A(x)\frac{\partial S}{\partial t} + \frac{\partial}{\partial x}(QS) = \frac{\partial}{\partial x}\left[K_x(x)A(x)\frac{\partial S}{\partial x}\right], \qquad (1)$$

where A is the local cross-sectional area and x is measured upstream from the mouth of the estuary, S is the salinity, Q is the river flow, and K_x is the longitudinal dispersion coefficient (Harleman and Thatcher 1974; Thatcher and Harleman 1981).

The longitudinal dispersion coefficient, K_x, is used to parameterize a variety of physical mechanisms, including tidal dispersion mechanisms that rely on either vertical or horizontal shear in tidal currents along with corresponding variations in salinity (e.g., Fischer et al. 1979). From a practical standpoint, most of these dispersion mechanisms give "reasonable" values of K_x, typically $O(100\ \mathrm{m^2\ s^{-1}})$, through appropriate (and reasonable) choices of the parameters that govern each mechanism (Fischer et al. 1979).

The variability of K_x can be important: For example, Garvine et al. (1992) described the response of salinities in the Delaware Estuary to flow as being "surprisingly weak." Given that solutions to (1) using constant values of K_x for the Delaware geometry overpredicted changes in salinity intrusion, they argued that K_x must increase with increasing river flow to produce the observed response.

Hansen and Rattray (1965) were the first to compute K_x using an analytical model of gravitational circulation. In the simplest case, divergence of the shear stress associated with a vertically sheared horizontal flow balances the baroclinic pressure gradient caused by the longitudinal salinity gradient. This gives a vertically sheared flow, U_g:

ν_t

where β is the saline expansivity, H is the local depth and ν_t is the eddy diffusion coefficient for momentum. The constant value of ν_t that one chooses must be that appropriate for the tidally averaged flow. For unstratified tidal flows ν_t is proportional to the rms tidal velocity. For stratified flows the absence of closures capable of properly reflecting the integrated effects of tidal variations in stratification and mixing (Stacey et al. 1999) becomes, in effect, a fitting parameter (Lung and O'Connor 1984; Uncles and Stephens 1990). For example, fitting ADCP-measured velocity profiles to Hansen and Rattray's theory, Monismith et al. (1996) found that ν_t inferred for subtidal flows through Carquinez Strait (Fig. 1) during a period of tidally varying stratification was approximately 1/20 of its value in unstratified flows of the same strength.

The salt balance appropriate to this flow is one in which a vertically varying salinity perturbation S' is created that represents a balance of horizontal advection of the mean gradient (dS/dx) by U_g and vertical diffusion of S'. As Hansen and Rattray (1965) show, this gives

$$K_x \sim \frac{(\beta g)^2 \left(\frac{dS}{dX}\right) H^8}{\nu_t^3}, \qquad (3)$$

where we have assumed that the vertical eddy diffusion coefficient for salt is equal to that of momentum, an assumption that is most accurate for unstratified flows (Fischer et al. 1979; Ivey and Imberger 1991). Generally, for unstratified flows, both ν_t and E_0 are proportional to H, so (3) is proportional to H^5. Assuming a triangular section, Fischer (1972) obtained a result similar to (3) excepting that the factor of H^8 was replaced by H^6W^2, where W is the width, and ν^3_t is replaced by $\nu^2_t E_0$, where E_0 is the diffusion coefficient for lateral momentum and scalar fluxes.

At steady state, the net flux of salt is zero (Hansen and Rattray 1965; MacCready 1999), so that

$$\frac{-Q}{A}S = K_x \frac{dS}{dx} = \frac{\alpha(\beta g)^2 H^8}{\nu_t^3}\left(\frac{dS}{dX}\right)^3, \qquad (4)$$

where $\alpha = 5.4 \times 10^{-5}$ is the constant of proportionality in (3). This can be rewritten as

$$\left(\frac{dS}{dX}\right)^3 = \frac{-Q\nu_t^3}{W\alpha(\beta g)^2 H^9} S, \qquad (5)$$

which in terms of the salinity intrusion length scale, X_s, gives

$$\frac{S_0}{X_s} \sim \frac{Q^{1/3}\nu_t S_0^{1/3}}{(W\alpha)^{1/3}(\beta g)^{2/3}H^3} \quad \text{or}$$

$$X_s \sim \frac{(W\alpha)^{1/3}(\beta g S_0)^{2/3}H^3}{Q^{1/3}\nu_t} \qquad (6)$$

for an estuary with constant W and H and with S_0 the ocean salinity. Thus X_s is proportional to $Q^{-1/3}$. This scaling applies in the limit where what Hansen and Rattray term the “diffusive fraction” of salt transport, that is, the percentage of the salt flux supported by mechanisms other than gravitational circulation, is zero. In this case, as the salinity distribution becomes more tightly compressed by net advection, the dispersive salt flux increases. This “stiffening” of the response of the salt field to large flows is referred to by Hansen and Rattray (1966) as an estuarine version of Le Chatelier's principle. Moreover, since ν_t is proportional to the rms tidal velocity, in the absence of tidal dispersion one would expect the scale of salinity intrusion to change throughout the spring–neap cycle. MacCready (1999) and others point out that two factors mitigate this effect: 1) Tidal dispersion tends to increase with tidal velocity (Zimmerman 1986), thus pushing more salt upstream at spring

tides than at neap tides; 2) the time required to significantly change the salt field from one state to another may be longer than the fortnight timescale of spring–neap variations.

How well is the scaling in (6) supported by observations? For the Hudson, Abood (1974) finds that $X_s \sim Q^{-1/3}$ holds for low flows and $X_s \sim Q^{-1}$ for high flows (see also Bowen 2000). The latter proportionality is what one finds if K_x is independent of dS/dx, that is, if none of the salt transport is associated with gravitational circulation. In contrast, Oey (1984) argues that the Hudson data are best described as following $X_s \sim Q^{-1/5}$, at least for all but the highest flow rates observed.

In this paper, we discuss the relation of salinity intrusions to flow in partially mixed estuaries using an extensive dataset of subtidal salinity variations in northern San Francisco Bay. We will show that the mean salinity distribution is nearly self-similar, allowing us to use X_2 (defined above) as an unambiguous flow-dependent length scale for salinity intrusion. Using over 20 years of data in which flow varies by a factor of approximately 200, we show that $X_2 \sim Q^{-1/7}$. We will argue that this weaker dependence of salinity intrusion on flow is due both to geometry of San Francisco Bay and the effects of stratification on vertical mixing.

2. Data sources

Several sets of data were used in our analysis: 1) CTD sections taken along the axis of northern San Francisco Bay roughly every two weeks by the United States Geological Survey (USGS) San Francisco Bay Project (e.g., Wienke et al. 1993; Cloern 1996); 2) long-term shore surface salinity stations maintained by the Bureau of Reclamation (Jassby et al. 1995); and 3) outflow estimates developed by the California Department of Water Resources. In sum total these data span more than 20 years in time. Because these years include severe droughts (1976–77) as well as very wet El Niño years (e.g., 1982), this dataset includes freshwater flow rates between (essentially) zero and 10 000 $m^3\ s^{-1}$.

a. Freshwater flow data

The measurement of freshwater flow is crucial to interpretation of the salinity data. In the Sacramento–San Joaquin Delta this is complicated by the fact that there are considerable withdrawals and return flows between the Bay and the gauged riverine inputs. The crux of the problem is that in the tidal delta there is the notable signal processing problem of extracting small mean flows from large tidal flows, thus rendering direct gauging of outflow impractical until recently (Oltmann 1999). Consequently, the California Department of Water Resources has developed a water balance analysis known as "DAYFLOW" that yields a number known as "Net Delta Outflow."[1] This balance uses gauged flow rates upstream of the delta, estimates of minor ungauged flows, flows at large state and federal pumping facilities in the southern delta, and measurements of precipitation and estimates of consumptive use within the delta. It is thought that computed flows are not very accurate, at least on a daily basis, for very low flow rates when the effective flow can actually be from the bay into the delta. This has been attributed to a spring–neap cycle of filling and emptying of the delta, the dynamics of which have yet to be explored.

b. Hydrographic data

The USGS data we used are from hydrographic sections taken along the channel of northern San Francisco Bay by the USGS San Francisco Bay project (e.g., Cloern 1996).[2] These data consist of a series of CTD drops taken at fixed stations approximately once per month. The sampling strategy is designed such that the sampling vessel, the USGS R/V *Polaris*, follows the flooding tide up through the bay. To compute average salinity from USGS data we numerically integrated the observed salinity distributions with depth, and X_2 estimates were produced by linearly interpolating between stations where the bottom salinity was greater than 2 psu and where it was less than 2 psu. We also used limited CTD transect data taken in 1986 by the USBR and processed as above.

The CTD transect data represent instantaneous profiles, and thus are aliased to some extent by tidal variations. Given maximal tidal excursions of 10 km, we estimate the amount of aliasing to be several kilometers at most; however, the data we present below, show that when distance is scaled by X_2, the scatter about the "standard" distribution is somewhat smaller than this, suggesting that the USGS sampling strategy better records the upstream/downstream displacement of the entire structure. The same would not be true for stratification which can vary substantially through the tidal cycle (Peters 1997; Geyer et al. 2000; Stacey et al. 1999).

c. USBR salinity station data

The computation of X_2 summarized in Jassby et al. (1995) made use of data taken by the USBR continuously between 1967 and 1991 at six monitoring locations. One exception to this was the 77-km station, which was replaced in 1978 by a similar station 75 km from the Golden Gate operated by the California Department of Water Resources (DWR). In general, all these stations sampled 1 m below the surface in about 10 m of water at a point between the shoreline and the ship channels.

The measurements were converted to salinity and corrected to bottom salinity assuming a constant top–bottom salinity difference of 0.24 psu determined from the mean of surface and bottom salinities measured from water samples taken with a Van Dorn sampler (referred to as "grab samples"). Examination of limited California Department of Fish and Game grab samples (top and bottom) during this period showed that near 2 psu at the bottom, stratification for the low salinity part of the estuary did not systematically depend on freshwater flow except at extremely high flows. Given the dynamic nature of stratification in partially mixed estuaries like San Francisco Bay, we expect that this assumption primarily increases the noise in the X_2 time series, although it may also give a systematic *downstream* bias to the X_2 estimate at very high flow rates when stratification can be significantly stronger than 0.24 psu. Clearly, from the perspective of evaluating the large-scale response this assumption seems adequate. A better estimate of X_2 (although not available retroactively) could be obtained by using a set of bottom salinity recorders.

A second problem with the historic data is that the original hourly data are no longer available in electronic format, forcing us to use the daily averages that were available. This may have introduced an erroneous cycle into the data with an approximately 14-day period. To examine this, we used more recent hourly data from the DWR Mallard Slough station and compared daily means of the raw data with data passed through a Godin tidal filter. In the end, the effects of this aliasing were very slight.

d. Computation of X_2 from USBR data

We sought to transform the data so that the salinity–distance relationship could be linearized around the 1–3-psu range to enable us to interpolate to get X_2 for each date. In order to mimic a local solution to the advection diffusion equation [Eq. (1)], we made a log regression of salinity as a function of distance, namely,

$$\ln(S) = b + cx/V_x \quad (7)$$

where b and c are constants and V_x is the mean upstream volume at a given location, thus interpolating log(S) versus x/V_x for each date in the sample series. In some cases we extrapolated, but did not do so beyond 5 km from the nearest station. Of a total of 8827 days in that series, we were able to obtain 7794 values from the interpolation. In most cases missing data arose either because X_2 was downstream of 56 km or because gaps appeared in data from a critical station. Data were interpolated separately for the Sacramento and San Joaquin Rivers. Data from the Sacramento River only were used when the value fell below 83 km (since there was a station at 81 km in the Sacramento, at about the confluence of the two rivers); when it was upstream of that point, the two values were averaged.

3. Results

a. Time and flow dependency of X_2

The response of the northern San Francisco Bay salt field to flow variations is typified by the behavior shown in Fig. 2, a plot of flows and low-pass filtered salinities at five stations spanning the entirety of the north bay for 1992.[3] The 1992 water year (which began 1 October 1991) was relatively dry. In this case it is clear that the salt field adjusted in a nearly simultaneous fashion to the large increase in flow that occurred ~ day 130.

This behavior is expressed in terms of X_2 in Fig. 3 where we plot the full time series of X_2 as well as the full time series (1967–90) of daily averaged flow. As discussed in Jassby et al. (1995) and above, this time series includes both interpolated X_2 values and, for periods of time when suitable interpolation could not be carried out because of missing data, hindcasts based on an autoregressive model of flow and X_2 developed by Alan Jassby (see Jassby et al. 1995). Jassby found that for daily values of X_2 the best fit to the observed data is the expression

$$= 2.50 \log_{10}[Q(t)], \quad (8)$$

where X_2 today (km), $X_2(t)$, depends on its value yesterday, $X_2(t-1)$, and the daily averaged flow ($m^3\ s^{-1}$). The value of R^2 for this expression was 0.986, and the standard error of the regression was 1.32 km for predicting each value using the previous predicted (rather than actual) value.

Because the theoretical predictions for salinity intrusion and flow involve power-law relations rather than logarithms, we recalculated a nonlinear fit between flow, $X_2(t)$, and $X_2(t-1)$. Using a standard least squares nonlinear regression routine (the Matlab proprietary software function "nlinfit"), we found that with a value of $R^2 = 0.98$,

$$X_2(t) = 0.919X_2(t-1) + 13.57Q^{-0.141}. \quad (9)$$

Analogous to a simple RC filter, (9) models a linear system that has a time constant of (1/0.081) = 12 days. Thus, the fundamental response times of the estuary is comparable to the fortnight timescale of the spring–neap cycle, and, to first order, is independent of flow.

An alternative to (9) is one in which the coefficient multiplying $X_2(t-1)$ depends on flow (Denton 1993). Assuming a linear relationship between this coefficient and flow (i.e., the simplest model possible), we found that the response time varied between 7 days at the highest flows and 11.3 days at the lowest flows. However, this more complicated model did not improve the fit to observations nor did it reduce autocorrelation of the residuals. While it is intuitively appealing that the response time should depend on flow (see MacCready 1999), the present dataset does not allow us to unambiguously demonstrate the connection.

To deduce the steady-state response, we set $X_2(t) = X_2(t-1)$ and find that

$$X_2 = 167Q^{-0.141}. \quad (10)$$

The uncertainty for the exponent is estimated to be (95% confidence level) ±0.005, although the real uncertainty is likely to be slightly larger because of a small degree of autocorrelation in the residuals. Thus, as shown in Fig. 4, the power-law exponent, obtained for more than 2½ decades of flow variation is −1/7 rather than −1/3. Evidently, the response of San Francisco Bay to high flow rates is much weaker than what would be expected using Hansen and Rattray's theoretical expression for K_x.

b. The spatial structure of the salt field

Samples of the USGS CTD data were plotted in Jassby et al. (1995). In Fig. 5, we plot this data for 1988–93, with salinity plotted as a function of X_2, showing a near-similarity form for salinity as a function of x/X_2. For values of $x/X_2 \approx 1$, the distribution appears to vary exponentially with distance toward the ocean, as expected for the simplest models of salinity intrusion. There is a central region of constant salinity gradient approximately given by

$$\partial S/\partial x \approx 37.5/X_2. \quad (11)$$

For typical values of $X_2 \approx 75$ km, (11) gives 0.5 psu km^{-1}. Near the Golden Gate, that is, $(x/X_2) \approx 0$, where the salinity approaches oceanic salinity, the gradient is much weaker. Evidently, the reduced salinity gradient near the Golden Gate reflects a larger dispersion coefficient due to greater depth and a reduced outward advection speed due to increased cross-sectional area found there.

At very high flow rates, this similarity appears to break down. An example of this behavior is seen in Fig. 6, a sequence of CTD sections taken in 1986 following the flood event of record which peaked on 20 February with a flow rate in excess of 17 000 $m^3\ s^{-1}$. The CTD sections start on 25 February (Q = 7900 $m^3\ s^{-1}$) and end 18 April, at which time the flow had dropped off to about 1200 $m^3\ s^{-1}$. They show how at very high flows the salinity at the Golden Gate is depressed substantially and in general that salinities in the bay are lower than what would be expected from the lower flow data. However, by the end of this period, equilibrium has been restored as has the more usual ~ 32 psu oceanic salinities at the Golden Gate.

A second excellent example of this behavior can be seen in Fig. 7, a plot of delta outflow flow and depth averaged salinity at the Golden Gate for the water year 1995 (1 October–30 September 1995). As seen in Fig. 7a, this year was

quite wet with an extended period of flow over 1000 $m^3 s^{-1}$. Consequently, salinity (Fig. 7b) at the Golden Gate was depressed below dry weather values for much of the winter and spring. The covariability of salinity and flow is shown in Fig. 7c, where it can be seen that salinity at the Golden Gate remained near 32 psu for flow less than about 1000 $m^3 s^{-1}$ and then dropped with increasing flow.

The USGS took CTD transects at roughly 1-month intervals during this period. Depth-averaged salinities scaled by salinity at the Golden Gate are plotted in Fig. 8, which shows a reasonable collapse of the salinities to the "universal" distribution. It is likely that the deviations from the base salinity distribution may be attributable to the more complex nature of flows in Central Bay under conditions of high outflow and strong stratification, when the Golden Gate region may be the site of internal hydraulic controls (Largier 1996). For these conditions, as seen in this data, one would not expect the simple 1D distribution to provide a complete description of the salinity field.

Finally, a test of the quality of our interpolated X_2 time series can be had by plotting all of the fixed station USBR data in terms of $S(x/X_2)$. The USBR data essentially fall on top of the USGS data with roughly the same degree of scatter (Fig. 9). Thus, we can place some confidence in X_2 obtained by interpolation.

c. Synthesis: Dispersion coefficients for northern San Francisco Bay

Assuming steady-state conditions,[4] we can use the USGS/USBR data to estimate the dispersion coefficient, K_x, which depends on both the position and flow. Suppose we have similarity,

$$S = S_0 f(x/X_2) = S_0 f(\xi): \quad (12)$$

then the steady-state condition of zero net salt flux implies that

$$K_x(x, Q) = \frac{-QX_2}{A(x)} \frac{f(\xi)}{\frac{df}{d\xi}(\xi)} = \frac{-QX_2}{A(x)} g(\xi), \qquad (13)$$

where the functions f, $df/d\xi$, and thus g, can be computed from the observations. Along with the observations, Fig. 6 includes a smooth spline fit to the observations. Because it is smooth, this spline fit can be differentiated easily.

Taken in conjunction with known values of $A(x)$ (Peterson et al. 1975; also see below), we can compute $K_x(Q)$ for each position x. For example, near $x/X_2 \approx 0$, $A(x) = 9 \times 10^4$ m^2. At this location when $Q = 100$ $m^3 s^{-1}$, $X_2 = 88$ km, giving $K_x \approx 600$ $m^2 s^{-1}$, which is larger than is typically cited for estuaries [200 $m^2 s^{-1}$: cf. discussion in Fischer et al. (1979)], particularly for tidal dispersion, but nonetheless is required for the salt balance. We summarize these results in terms of the spatial variation in K_x for different values of Q in Fig. 10. It is clear that for any fixed location, the range of K_x is substantial and increases monotonically with flow rate. Values of K_x comparable to those we report here (i.e, ~ 2000 $m^2 s^{-1}$) have also been deduced from salinity data for Delaware Bay by Garvine et al. (1992).

4. Numerical model of salinity intrusion

One concern in applying simple scaling models of salinity intrusion to San Francisco Bay is that neither the depth nor the cross-sectional area is constant. For reference, the cross-sectional area and the depth, taken from Peterson et al. (1975), are plotted in Fig. 11. The scaling arguments given in the introduction assume constant area and constant depth. If these vary, as is the case in San Francisco Bay, the scaling of flow and salt intrusion length may deviate from theoretical predictions even if the physical basis of the scaling is correct. Accordingly, to test the importance of variations in geometry on the flow–salinity relationship, we numerically integrated (4), modified to include a constant, base value of the dispersion coefficient, K_B; that is,

$$K_B \frac{dS}{dx} + \frac{\alpha(\beta g)^2 H^5}{\gamma^3 u_*^3} \left(\frac{dS}{dX}\right)^3 = \frac{-Q}{A} S. \qquad (14)$$

Equation (14) also assumes that v_t appearing in (4) can be written as $\gamma u_* H$, where γ is the turbulent mixing coefficient made dimensionless by Hu_*. For example, in homogeneous flows, $\gamma \approx 0.1$ (Fischer et al. 1979). Depths and cross-sectional areas were taken from Peterson et al. (1975). Salinity at the Golden Gate was assumed to vary with flow as seen in Fig. 7c. For the sake of this simple modeling exercise, appropriate values were derived by fitting a curve by eye to the data and Fig. 7c, and reading the appropriate value of salinity corresponding to the flow chosen. The shear velocity was set to 2 cm s^{-1}, a value typical of rms tidal currents in northern San Francisco Bay (Stacey et al. 1999).

The model expressed in (14) has two free parameters, K_B and γ. While their values can be estimated crudely from the literature, the accuracy of predictions of salinity or of X_2–Q relations will depend on specific choices of K_B and γ. For example, in Fig. 12, we plot $X_2(Q)$ computed for $\gamma = 0.02$ and $K_B = 25$, 50, 100, and 200 m^2 s^{-1}, along with best fit to observations given by (10). The power-law exponents derived from fitting $X_2 \sim Q^n$ for each these computed cases range from −0.21 for $K_B = 25$ m^2 s^{-1} to −0.29 for $K_B = 200$ m^2 s^{-1}; that is, these all show more sensitivity of X_2 to flow than we observe.

Alternatively, one can choose both parameters so as to best match observations. In doing so, we found that with smaller values of γ we could match the high flow response, but tended to overpredict X_2 at low flows. Thus, with fixed values of γ the behavior appears as shown in Fig. 12, that is, closer to the $Q^{-1/3}$ behavior predicted by Hansen and Rattray than to the $Q^{-1/7}$ behavior observed. This suggests allowing γ to vary with flow. We chose $K_B = 30$ m^2 s^{-1}, a value that falls within the acceptable range of tidal dispersion coefficients, and then solved for γ that best matched observations. These results are reported in Table 1, where it appears that as flow increases, γ decreases, presumably reflecting the effects of increasing density stratification. This approach parallels that of Harleman and Thatcher (1974), although they chose to set $K_x \propto \partial S/\partial x$, with an experimentally derived stability and flow dependent constant of proportionality. In our case, even at the lowest flows, the values of v_t implied are 1/25 of their homogeneous values; this gives an amplification of K_x over its value for homogeneous conditions of $25^3 \approx 16\,000$. At the highest flow rate we examined, the 20-fold reduction in v_t (as compared with homogeneous conditions) corresponds to an inflation of K_x by a factor of 50 000.

Using $K_B = 30$ m^2 s^{-1} and the values of γ given in Table 1, the spatial structure of the computed salinity fields, plotted as a function of x/X_2 (Fig. 13) is in excellent agreement with the nearly self-similar form that is observed. Thus, while it requires some degree of empiricism, the 1D advection–diffusion model shows that both spatial structure and response to flow are reproducible if we use real bathymetry and allow vertical exchange coefficients to decrease with increased flow and hence decreased salinity intrusion.

A two-layered model of salinity in San Francisco Bay has been presented in Uncles and Peterson (1996). In their model, salt flux due to gravitational circulation is handled explicitly by means of the vertically sheared subtidal flows in each layer. Importantly, turbulent mixing rates are assumed not to depend on stratification. As we find above, in the absence of stratification, predictions of X_2 are too small at high flow rates. Thus, we conclude that it is essential to include the tendency of stratification to reduce vertical mixing in order to model salinity intrusion. To remove the effects of variable bathymetry on the computed X_2 relation, we reran the model using average bathymetry but the same Q-dependent values of γ, finding that the effects of stratification alone give $X_2 \sim Q^{-1/6}$, a law somewhat closer than is $Q^{-1/3}$ to the $Q^{-1/5}$ fit found by Oey (1984) for the Hudson, an estuary that has approximately constant cross section.

Changes in stratification with river flow appear to play a pivotal role in the dynamics of the salt field. According to Fischer (1972), salinity intrusion and stratification are expected to depend on the estuarine Richardson number,

$$\mathrm{Ri}_E = \beta S_0 g Q / W U^3,$$

such that the transition from strongly stratified to well mixed conditions should take place for $0.08 < \mathrm{Ri}_E < 0.8$. We have converted our flow rates into equivalent values of Ri_E using a typical width of 2100 m and a value of the rms tidal velocity $U = 0.6$ m s^{-1}. The computed values of γ, as well as the change in salinity with flow at the Golden Gate suggest that the transition takes place for flows somewhere between 300 and 1000 m^3 s^{-1}, or for values of $\mathrm{Ri}_E \approx 0.03$. However, it is worth noting that even for very small values of Ri_E, stratification effects seem important, behavior that we attribute to the

tidally varying stratification observed even at low flow rates (Monismith et al. 1996; Stacey et al. 2001).

This connection between stratification and Ri_E is illustrated in Fig. 14 where several sets of salinity stratification data have been plotted as a function of Ri_E. Data from northern San Francisco Bay consist of top − bottom salinity differences, ΔS, averaged along the estuary for USGS transects from all of 1988–93 and from the winters 1996/97 and 1998/99. The latter two datasets have been included because both winters were quite wet. Ri_E for this data was computed using 15-day averages of the inflow. Figure 14 also includes data taken from Fisher (1972, see references therein) for various estuaries around the world. While there is substantial scatter, as might be expected given the tidal timescale dynamics responsible for stratification evolution (Simpson and Sharples 1991; Stacey et al. 2001), ΔS is generally larger for larger values of Ri_E. Because of the scatter in the data, we have not attempted a power-law fit of $\Delta S/S$ as a function of Ri_E. Nonetheless, it appears that the actual dependence might fall somewhere between the $Ri_E^{1/3}$ suggested by Oey (1984) and $Ri_E^{1/2}$.

Finally, we note that it might also possible to match $X_2(Q)$ by choosing K_B so that it varies with x. For example, Hansen and Rattray (1965) showed that to have a similarity solution to their equivalent of (14) they had to choose dK_B/dx to be proportional to the local cross-sectionally averaged mean velocity, that is, to the freshwater flow. In general, given the wide variety of mechanisms that can bring about dispersion even in the absence of buoyancy effects (see Fischer et al. 1979) this assumption, while facilitating the analysis, hardly seems warranted. Moreover, since K_B is taken to represent primarily tidal dispersion mechanisms, it should not be easily related to freshwater inflow. However, for San Francisco Bay, the plots of $K(x, Q)$ given in Fig. 10 show clearly that no single value of K_B would match the 30-fold variation in K_x with flow inferred to exist throughout northern San Francisco Bay.

5. Discussion: The effects of tidally varying stratification on salt flux

The observations and modeling shown above make clear that the salt balance in northern San Francisco Bay can only be predicted using the simple physics embodied in the Hansen–Rattray model of gravitational circulation if, as suggested by Garvine et al. (1992), the mixing coefficients vary with flow. Thus, while the Hansen–Rattray model is qualitatively correct, it does not allow us to predict quantitatively how the depth-averaged salinity field responds to flow. Indeed, Hansen and Rattray recognized the empiricism inherent to choosing suitable vertical mixing coefficients and chose them so as to best match the limited data available at the time. In the present case, the enormous range of flows to which San Francisco Bay is exposed allows us to systematically evaluate how these effective mixing coefficients, which are in reality the net effect of complex tidal variations in turbulence structure (Stacey et al. 1999), vary systematically with river flow for *one* estuary. It seems unlikely that the particular values of K_B or γ derived from the San Francisco Bay data are directly applicable to other estuaries. However, in what follows we argue that the our result that increasing river flow leads to decreases in the effective tidally averaged vertical mixing rates and hence increases in upstream salt flux is broadly applicable to partially stratified estuaries.

The dependence of mixing on flow must reflect changes in stratification that result when the salinity gradient intensifies (Simpson and Sharples 1991). As laid out by Simpson and colleagues (Simpson et al. 1990; Simpson and Sharples 1991; Sharples et al. 1994), there appears to be two states for partially mixed estuaries—one with strain-induced periodic stratification (SIPS) and one where the stratification intensifies with time, a mode they describe as runaway stratification. Monismith et al. (1996) (also Stacey 1996; Bowen 2000) found that this transition is best described by the horizontal Richardson number

$$\mathrm{Ri}_x = \frac{g\beta\dfrac{dS}{dx}H^2}{u_*^2}. \qquad (15)$$

When $Ri_x < Ri_{crit}$ where the critical value of Ri_x, Ri_{crit}, is an $O(1)$ constant, mixing is strong and periodic stratification results, whereas when $Ri_x > Ri_{crit}$, mixing is not sufficient to prevent the development of stratification that intensifies each tidal cycle. Note that because the longitudinal salinity gradient, dS/dx, depends on flow, ultimately, the transition criteria can be related to Ri_E (Bowen 2000).

The critical value of Ri_{crit} has been found to be ~ 0.3 from modeling (Monismith et al. 1996; Bowen 2000) using the Mellor–Yamada 2.5 closure (Blumberg et al. 1992) and 0.6 from observation (Monismith et al. 1996; Stacey 1996). The

difference may be due to the fact that Mellor–Yamada closure used in the 1D model tends to overpredict the effects of stratification on vertical mixing (Stacey et al. 1999).

Most important is that this transition between stratification states dramatically changes the upstream salt flux. To make this point we present limited observations of salt flux made in Suisun Cut in northern San Francisco Bay during 1995 (see Stacey et al. 1999). The upstream salt flux (measured using an ADCP and a collocated CTD) at the bottom increases strongly when Ri_x (computed using the ADCP and the horizontal density gradient computed using two fixed stations in the Suisun Cut channel) surpasses its critical value (Fig. 15). Further discussion of these observations will be reported elsewhere. These observations are similar to ones shown in Bowen (2000) for the Hudson estuary.

Using these ideas we can formulate an alternative dynamic equilibrium model for the salt field: For a given flow the salt field goes through the transition from SIPS to runaway stratification for some part of the spring–neap cycle depending on time of year (because of variations between tides at equinoxes). During the runaway state, K_x is much larger than during the SIPS part of the cycle so that the effective K_x that acts to produce the quasi-steady response documented above is the result of combining a low background upstream salt flux with a short intense pulses of upstream salt flux. If the flow rate increases, the salt field starts to compress, intensifying dS/dx, which acts to increase Ri_x and thus increase the likelihood of transition to runaway stratification and hence increases the fraction of the spring–neap cycle for which K_x is large. The larger the flow, the greater the fraction of time K_x is large. Thus, the negative feedback (upstream salt flux) intensifies as the forcing intensifies, thus blunting the response of the salt field to large flows. As seen in section 4, this tidal timescale physics can evidently be mimicked by a reduction in vertical exchange coefficients used to model subtidal salt flux.

To look at the dependence of K_x on Ri_x, we ran the one-dimensional estuarine water column model discussed in Lucas et al. (1998) (see also Simpson and Sharples 1991; Bowen 2000) to compute K_x for the case where mixing coefficients vary with stratification, and runaway stratification can occur. This model, which is based on the one-dimensional version of the Princeton Ocean Model used by Blumberg et al. (1992), solves the unsteady momentum and salt balances for a horizontally homogeneous, vertically variable water column. It includes a constant amplitude M_2 tidal pressure gradient, a baroclinic pressure gradient due to a constant horizontal salinity gradient, and computes turbulent mixing coefficients using the version of the Mellor–Yamada level-2.5 closure presented by Galperin et al. (1988).

Using the tidally varying salt and velocity fields we can compute depth-integrated horizontal salt fluxes, from which K_x can be computed by dividing through by the salinity gradient. The results of this calculation are shown in Fig. 16 (for H = 10 m) where we have normalized K_x by $u_* H$. It is easily shown that the Hansen and Rattray K_x for homogeneous water columns (with $\nu_t = 0.1\, H u_*$) so nondimensionalized is

$$K_x/u_* H = 5.5 \times 10^{-2} \mathrm{Ri}^2_x. \quad (16)$$

The results of our computation show this power-law dependency, albeit with a constant that is 10^4 times larger than would predicted (presumably an effect of stratification), for subcritical values of Ri_x whereas it jumps about a factor of 40 and is constant for Ri_x greater than the critical value of 0.5. Bowen (2000) reports similar computations that also show a jump in K_x for supercritical Ri_x.

To use this result to examine the idea of a dramatic increase in salt flux with transitions during the spring–neap cycle from SIPS to runaway stratification states, we used the depth-averaged tidal currents from Carquinez for February–March 1991 [the data discussed in Monismith et al. (1996)] to provide an appropriate time variation in u_*. Using Fig. 16, we computed K_x at each time through the spring–neap cycle and average over the entire 30-day period. The results of this are shown in Fig. 17, for H = 10 m and H = 20 m. For the 10-m case, the amplitudes of the tidal currents were adjusted to 75% of the observed values, roughly reflecting the difference in tidal currents between 10-m water columns in Suisun Bay and the 20-m-deep Carquinez Strait.

Although it reflects a rather crude model of the real physics, this plot shows a region in which the stratification never "runs away" and for which $K_x \propto (dS/dx)^2$; a region in which the the stratification runs away some of the time, K_x increases dramatically with small changes in (dS/dx), and finally a range in which K_x may be constant. Thus, the dependence of K_x on (dS/dx) defines three regimes of estuarine dynamics [albeit translated from salinity gradient to flow as per Bowen (2000)]: 1) At very low flow rates, the Hansen–Rattray scaling prevails and salinity intrusion should follow the $Q^{-1/3}$ behavior this

scaling provides for uniform channels; 2) at moderate flow rates, salinity flux jumps dramatically when the critical value of Ri_x is exceeded; 3) at high flow rates, the salinity structure is nearly two-layered. As suggested by Geyer et al. (2000), the upstream salt flux may then be limited by friction in the lower layer. In this regime, the Q^{-1} dependence of salinity intrusion found by Abood (1974) for high flow follows from constancy of K_x. As discussed by Stommel and Farmer (1953), hydraulic controls may also limit landward salt flux.

In the middle regime no single power law can describe the relationship between K_x and (dS/dx). By varying the critical value of Ri_x, C_d, H, etc., one can change the value of dS/dx at which K_x jumps, and thus how wide a range of values of dS/dx fall in the transitional region. In reality, salinity gradients in northern San Francisco Bay are always in the range of 0.3–0.8 psu km^{-1}, and one might anticipate that for a small range of salinity gradients, as we observe, a single power law might serve as an adequate representation of the variation in K_x with salinity gradient. Perhaps more important, the values of K_x given in Fig. 17 are still smaller than the values we have inferred from observed salinities. This may reflect the effects of cross-sectional variations in flow structure and salt flux. For example, Fischer's analysis of K_x inflates the Hansen and Rattray value of K_x by a factor of $(W/H)^2$. Presumably the more complex and subtle interactions of lateral variations in salinity and possibly lateral frontogenesis may play an important role in determining how longitudinal salt flux is tied to flow conditions (O'Donnell 1993; Valle-Levinson and O'Donnell 1996).

For the present, our simplified view of the physics suggests that both geometry and the dynamic nature of stratification and salt flux may explain the weak flow dependence of salinity intrusion in northern San Francisco Bay. More generally, our model calculations allow us to speculate that three regimes of salinity intrusion may exist in nature: one satisfying Hansen–Rattray scaling, that is, the low-flow behavior observed in the Hudson; one observed in San Francisco Bay in which salt flux depends sensitively on salinity gradient and hence salinity intrusion is weakly related to flow; and finally, a regime in which upstream salt flux is proportional to the salinity gradient, and hence as observed in the Hudson for high flow rates salinity intrusion is strongly related to flow. Presumably, these transitions should be delineated by particular values of, Ri_E, the estuarine Richardson number (Fischer et al. 1979; Bowen 2000).

From the practical standpoint of making predictions of salinity intrusion using vertically resolved circulation models, it appears that the accuracy with which the turbulence closure models the effects of stratification may be important. If the model overpredicts the effects of stratification, as does the popular Mellor–Yamada level-2.5 closure (Stacey et al. 1999), then it will show too much upstream salt flux and hence will overpredict salinity intrusion. Conversely, if the closure underpredicts the effects of stratification, it will predict too little salinity intrusion.

6. Summary and conclusions

Long-term salinity data for northern San Francisco Bay show that depth-averaged salinity appears to be nearly self-similar, something that allows us to easily infer the way longitudinal dispersion coefficients depend on flow and position. This similarity facilitates the use of a single length scale, X_2, the distance from the ocean of the 2-psu isohaline, to describe how salinity intrusion depends on flow rate. Most importantly, we find that the length of salinity intrusion in northern San Francisco Bay is relatively insensitive to flow, behavior we attribute to the dynamic nature of tidal variations in stratification. We hypothesize that differences in the dependence of salinity intrusion on flow observed for different estuaries and different flow rates reflect differences in stratification and hence in stratification-induced reductions in vertical mixing rates.

Acknowledgments

We wish to thank all of the San Francisco Bay research community who made their data available to us, particularly Jim Cloern, Jim Arthur, Ralph Cheng, Rick Oltmann, and Larry Smith. Collection of these data has been supported by the USGS, the U.S. Bureau of Reclamation, and by the California Department of Water Resources. It is a pleasure to recognize the support given by NSF (OCE-9416604), the EPA (CE009605-01-0), and DWR to SGM. JRB is supported by the USGS and the Interagency Ecological Program. The authors wish to acknowledge the helpful comments provided to us by Parker MacCready and an anonymous reviewer.

REFERENCES

Abood K. A., 1974: Circulation in the Hudson estuary. *Hudson River Colloquium*, O. A. Roels, Ed., *Annals of the New York Academy of Science*, Vol. 250, NY Academy of Science, 38–111.

Blumberg A. F., B. Galperin, and D. J. O'Connor, 1992: Modeling vertical structure of open channel flows. *J. Hydraul. Div., ASCE*, **118**, 1119–1134. Find this article online

Bowen M. M., 2000: Mechanisms and variability of salt transport in partially stratified estuaries. Ph.D. thesis, Woods Hole/Massachusetts Institute of Technology Joint Program in Physical Oceanography, 171 pp.

Cloern J. E., 1996: Phytoplankton bloom dynamics in coastal ecosystems: A review with some general lessons from sustained investigation of San Francisco Bay, California. *Rev. Geophys.*, **34**, 127–168. Find this article online

Denton R. A., 1993: Accounting for antecedent conditions in seawater intrusion modeling—applications for the San Francisco Bay–Delta. *Hydraulic Engineering '93*, H. W. Shen, S. T. Su, and F. Wen, Eds., ASCE, 448–453.

Fischer H. B., 1972: Mass transport mechanisms in partially stratified estuaries. *J. Fluid. Mech.*, **53**, 671–687. Find this article online

Fischer H. B., E. J. List, J. Imberger, R. C. Y. Koh, and N. H. Brooks, 1979: *Mixing in Inland and Coastal Waters*. Academic Press, 483 pp.

Galperin B., L. H. Kantha, S. Hassid, and A. Rosati, 1988: A quasi-equilibrium turbulent energy model for geophysical flows. *J. Atmos. Sci.*, **45**, 55–62. Find this article online

Garvine R. W., R. K. McCarthy, and K. C. Wong, 1992: The axial salinity distribution in the Delaware Estuary and its weak response to river discharge. *Estuarine Coastal Shelf Sci.*, **35**, 157–165. Find this article online

Geyer W. R., J. H. Trowbridge, and M. M. Bowen, 2000: The dynamics of a partially mixed estuary. *J. Phys. Oceanogr.*, **30**, 2035–2048. Find this article online

Hansen D. V., and M. Rattray Jr.,, 1965: Gravitational circulation in straits and estuaries. *J. Mar. Res.*, **23**, 104–122. Find this article online

Hansen D. V., and M. Rattray Jr.,, 1966: New dimensions in estuary classification. *Limnol. Oceanogr.*, **11**, 319–326. Find this article online

Harleman D. R. F., and M. L. Thatcher, 1974: Longitudinal dispersion and unsteady salinity intrusion in estuaries. *La Houille Blanche*, **1/2**, 25–33. Find this article online

Ivey G. N., and J. Imberger, 1991: On the nature of turbulence in a stratified fluid. Part 1: The energetics of mixing. *J. Phys. Oceanogr.*, **21**, 650–658. Find this article online

Jassby A. D., W. M. Kimmerer, S. G. Monismith, C. Armor, J. E. Cloern, T. M. Powell, J. Schubel, and T. Vendlinski, 1995: Isohaline position as a habitat indicator for estuarine resources: San Francisco Bay–Delta, California, U.S.A. *Ecol. Appl.*, **5**, 272–289. Find this article online

Kranenburg C., 1986: A time scale for long-term salt intrusion in well-mixed estuaries. *J. Phys. Oceanogr.*, **16**, 1329–1331. Find this article online

Largier J., 1996: Hydrodynamic exchange between San Francisco Bay and the ocean: The role of ocean circulation and stratification. *San Francisco Bay: The Ecosystem*, T. Hollibaugh, Ed., American Association for the Advancement of Science, 69–104.

Lucas L., J. E. Cloern, J. R. Koseff, S. G. Monismith, and J. K. Thompson, 1998: Does the Svedrup critical depth model explain blooms in the coastal zone? *J. Mar. Res.*, **56**, 375–415. Find this article online

Lung W. S., and D. J. O'Connor, 1984: Two-dimensional mass transport in estuaries. *J. Hydraul. Eng.*, **110**, 1340–1357. Find this article online

MacCready P., 1999: Estuarine adjustment to changes in river flow and tidal mixing. *J. Phys. Oceanogr.*, **29**, 708–726. Find this article online

Monismith S. G., J. Burau, and M. Stacey, 1996: Stratification dynamics and gravitational circulation in northern San Francisco Bay. *San Francisco Bay: The Ecosystem*, T. Hollibaugh, Ed., American Association for the Advancement of Science, 123–153.

O'Donnell J., 1993: Surface fronts in estuaries: A review. *Estuaries*, **16**, 12–39. Find this article online

Oey L. Y., 1984: On steady salinity distribution and circulation in partially mixed and well mixed estuaries. *J. Phys. Oceanogr.*, **14**, 629–645. Find this article online

Oltmann R. N., 1999: Measured flow with tracer-dye data for spring 1997 and 1998 for the South Sacramento–San Joaquin Delta, California. *Interagency Ecological Program Newsletter*, Vol. 12, No. 8, 37–43.

Peters H., 1997: Observations of stratified turbulent mixing in an estuary: Neap-to-spring variations during high river run-off. *Estuarine Coastal Shelf Sci.*, **45**, 69–88. Find this article online

Peterson D. H., T. J. Conomos, W. W. Broenkow, and P. C. Doherty, 1975: Location of the non-tidal current null zone in northern San Francisco Bay. *Estuarine Coastal Mar. Sci.*, **3**, 1–11.

Schubel J. R., Coauthors, 1992: Managing freshwater discharge to the San Francisco Bay/Sacramento–San Joaquin Delta Estuary: The scientific basis for an estuarine standard. Rep. to the EPA, 109 pp.

Sharples J., J. H. Simpson, and J. M. Brubaker, 1994: Observations and modeling of periodic stratification in the Upper York River Estuary, Virginia. *Estuarine Coastal Shelf Sci.*, **38**, 301–312. Find this article online

Simpson J. H., and J. Sharples, 1991: Dynamically-active models in the prediction of estuarine stratification. *Dynamics and Exchanges in Estuaries and the Coastal Zone*, D. Prandle, Ed., Springer-Verlag, 101–113.

Simpson J. H., J. Brown, J. Matthews, and G. Allen, 1990: Tidal straining, density currents, and stirring in the control of estuarine stratification. *Estuaries*, **13**, 125–132. Find this article online

Stacey M. T., 1996: Turbulent mixing and residual circulation in a partially stratified estuary. Ph.D. thesis, Dept. of Civil Engineering, Stanford University, 209 pp.

Stacey M. T., S. G. Monismith, and J. R. Burau, 1999: Observations of turbulence in a partially stratified estuary. *J. Phys. Oceanogr.*, **29**, 1950–1970. Find this article online

Stacey M. T., J. R. Burau, and S. G. Monismith, 2001: The creation of residual flows in a partially stratified estuary. *J. Geophys Res.*, **106** (C8), 17013–17038. Find this article online

Stommel H., and H. G. Farmer, 1953: Control of salinity in an estuary by a transition. *J. Mar. Res.*, **12**, 12–20. Find this article online

Thatcher M. L., and D. R. F. Harleman, 1981: Long-term salinity calculation in Delaware Estuary. *J. Environ. Eng. Div., ASCE*, **107**, 11–27. Find this article online

Uncles R. J., and J. A. Stephens, 1990: The structure of vertical current profiles in a macrotidal partly mixed estuary. *Estuaries*, **13**, 349–361. Find this article online

Uncles R. J., and D. H. Peterson, 1996: The long term salinity field in San Francisco Bay. *Cont. Shelf Res.*, **15**, 2005–2039. Find this article online

Valle-Levinson A., and J. O'Donnell, 1996: Tidal interaction with buoyancy driven flow in a coastal plain estuary. *Buoyancy Effects on Coastal and Estuarine Dynamics*, D. Aubrey, Ed., Coastal and Estuarine Studies, Vol. 53, Amer. Geophys. Union, 265–281.

Wienke S. M., B. E. Cole, J. E. Cloern, and A. E. Alpine, 1993: Plankton studies in San Francisco Bay. XIV. Chlorophyll distributions and hydrographic properties in San Francisco Bay, 1992. U.S. Geological Survey Open-File Rep. 93-423, 175 pp.

Williams P. B., and J. T. Hollibaugh, 1989: A salinity standard to maximize phytoplankton abundance by positioning the entrapment zone in Suisun Bay. Phillip Williams and Associates Rep. 412-4, 35 pp.

Zimmerman J. T. F., 1986: The tidal whirlpool: A review of horizontal dispersion by tidal and residual currents. *Neth. J. Sea Res.*, **20**, 133–154. Find this article online

---

APPENDIX

7. Effects of Unsteadiness on Dispersion Coefficient Estimates

As discussed by Kranenburg (1986) and MacCready (1999), unsteadiness can play an important role in estuarine dynamics. Kranenburg's (1986) analysis points out that unsteadiness is significant when the freshwater flow changes more quickly than the estuary can respond. In the case of northern San Francisco Bay, the empirically defined time constant of the response of the salt field to changes in river flow is approximately 2 weeks. Flows into San Francisco Bay generally vary seasonally: spectral analysis shows that virtually all of the energy in the flow variability is at periods longer than 14 days. Hence, from the standpoint of Kranenburg's analysis, most of the variability in the salt field in northern San Francisco Bay can be modeled using a quasi-steady approach.

Nonetheless, the likely importance of unsteadiness to the salt balance used in this paper can be estimated using the self-similar form give in (12). Assume for now that S_0 is independent of flow, then

$$\frac{\partial S}{\partial t} = -S_0 \frac{df}{d\xi} \frac{x}{X_2^2} \frac{dX_2}{dt}. \qquad \text{(A1)}$$

In a similar fashion we can compute

$$u \frac{\partial S}{\partial x} = \frac{-Q_f}{A(x)} \frac{S_0}{X_2} \frac{df}{d\xi}. \qquad \text{(A2)}$$

Thus, to estimate the importance of unsteadiness, we can compute the ratio of these two terms using the observed time series for Q_f and X_2; that is,

$$\frac{\dfrac{\partial S}{\partial t}}{u \dfrac{\partial S}{\partial x}} = \frac{A(x)x}{Q_f X_2} \frac{dX_2}{dt} \approx \frac{10^9}{Q_f X_2} \frac{dX_2}{dt}, \qquad \text{(A3)}$$

where we have used a maximum value of the product $A(x)x \approx 10^9$ m^3. The absolute value of (A3) is plotted in Fig. A1, where it can be seen that the ratio appears to be $O(1)$ for much of the time when Q_f is small (Fig. A1a) and X_2 is large (Fig. A1b). This may be attributed to the fact that the time series of X_2 and Q_f are noisy. In particular, because the X_2 time series was rounded to the nearest kilometer, small changes in X_2 can lead to 1 km day^{-1} changes in X_2, which, at low flows, lead to values of the absolute value of 16 that are $O(1)$. If we use low-pass filtered versions of the X_2 and Q_f time series, the importance of unsteadiness as computed by 16 is reduced by a factor of 10–100, with the unsteady term generally being 1%–10% as large as the advective term. Clearly, the present dataset is not of sufficient accuracy to refine this analysis further.

Finally, in terms of the salt balance used to infer dispersion coefficients [cf. (13)] this formulation shows that the effect of unsteadiness on computed dispersion coefficients is proportional to dX_2/dt. Raw and filtered versions of dX_2/dt are plotted in Fig. A2, where the "bit noise" like nature of the daily changes in X_2 is evident. Most importantly, dX_2/dt mostly changes sign every few days. Hence it is likely that there is no *systematic* error in our dispersion coefficients; instead, unsteadiness primarily contributes uncertainty to our computed dispersion coefficients.

Tables

Table 1. Flow and mixing reduction

Flow (m^3 s^{-1})	R_R	γ
100	4.8×10^{-3}	0.0041
300	1.5×10^{-2}	0.0040
1000	4.9×10^{-2}	0.0036
3000	1.5×10^{-1}	0.0031
10 000	4.9×10^{-1}	0.0027

Click on thumbnail for full-sized image.

Figures

Click on thumbnail for full-sized image.

FIG. 1. Northern San Francisco Bay (plotted with software provided by R. Signell). The numbers mark different distances (km) from $x = 0$ at the Golden Gate

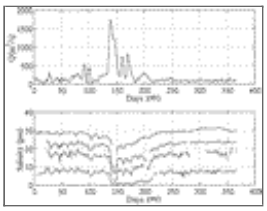

Click on thumbnail for full-sized image.

FIG. 2. Flow and salinity variability in 1993 in northern San Francisco Bay. The four salinity stations shown are located at x = 19.4, 40.5, 50.5, and 72.5 km

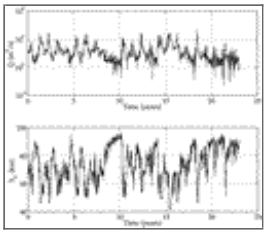

Click on thumbnail for full-sized image.

FIG. 3. Daily time series of river flow and salinity intrusion length scale X_2. The data series starts on 1 Oct 1967

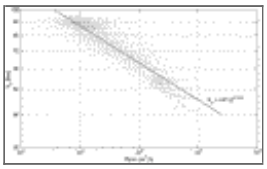

Click on thumbnail for full-sized image.

FIG. 4. Functional relationship between river flow, Q, and X_2. The line shown is the steady-state best-fit Q–X_2 relation given by Eq. (10)

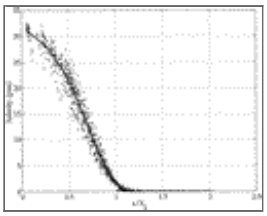

Click on thumbnail for full-sized image.

FIG. 5. Depth-averaged salinity as a function of x/X_2; X_2 was determined directly from bottom salinity measurements; data taken from USGS CTD transects 1988–92

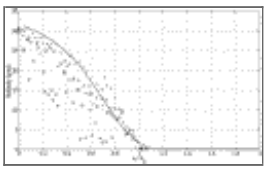

Click on thumbnail for full-sized image.

FIG. 6. An example of non-self-similar salinity distributions from Feb–Apr 1986 (data from USGS/USBR). Symbols represent: (◇) 25 Feb, $Q = 7900\ m^3\ s^{-1}$; (□) 20 Mar, $Q = 4700\ m^3\ s^{-1}$; (○) 25 Mar, $Q = 3200\ m^3\ s^{-1}$; (×) 8 Apr, $Q = 1900\ m^3\ s^{-1}$; (+) 18 Apr, $Q = 1200\ m^3\ s^{-1}$

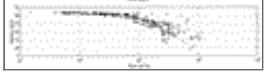

Click on thumbnail for full-sized image.

FIG. 7. Flows and salinity at the Golden Gate for water year 1995

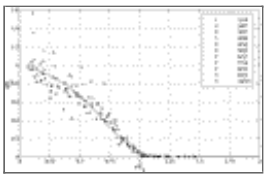

Click on thumbnail for full-sized image.

FIG. 8. Salinity distributions from water year 1995. Dates corresponding to symbols are shown on plot. The solid line is the dimensionless function derived from the spline fit to the 1988–93 data with the salinity at $x = 0$ scaled by the corresponding salinity at the Golden Gate

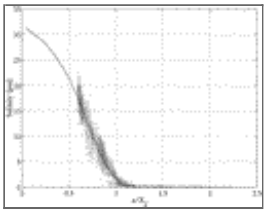

Click on thumbnail for full-sized image.

FIG. 9. USBR salinity data from four stations 1967–91 compared with unscaled salinity as a function of (x/X_2) found in 1988–93 USGS CTD transects

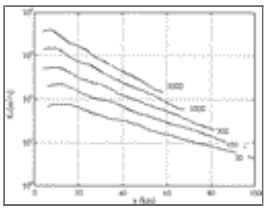

Click on thumbnail for full-sized image.

FIG. 10. Plot of $K_x(\mathrm{m}^2\ \mathrm{s}^{-1})$ as a function of position in the estuary for five different flow rates $(\mathrm{m}^3\ \mathrm{s}^{-1})$

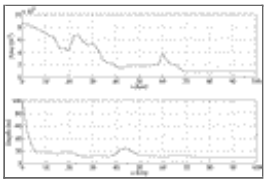

Click on thumbnail for full-sized image.

FIG. 11. Geometry of northern San Francisco Bay (taken from Peterson et al. 1975)

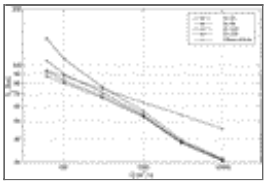

Click on thumbnail for full-sized image.

FIG. 12. Steady-state X_2–Q relations computed numerically using different values of K_B and keeping γ constant compared with observed values

Click on thumbnail for full-sized image.

FIG. 13. Computed salinity distributions as functions of distance from the Golden Gate normalized by $X_2(Q)$ for $K_B = 30\ m^2\ s^{-1}$ and with γ varying between 0.081 and 0.054 depending on flow. The (+) represent computed salinities for flows between 100 and 10 000 $m^3\ s^{-1}$, the (○) represent USGS observations, and the solid line is the spline fit to the USGS data

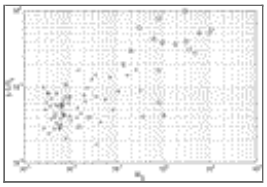

Click on thumbnail for full-sized image.

FIG. 14. Effect of Ri_E on estuarine stratification. Data taken from USGS CTD transects are the average along transect of top − bottom salinity difference for USGS from (+) 1988–93, (○) 1996–97, and (◇) 1998–99. Other data are taken from Fischer (1972) and represent the Vellar (□), the Gironde (△), and the Mersey (▽) estuaries

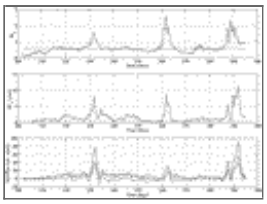

Click on thumbnail for full-sized image.

FIG. 15. Salt flux and stability in Susiun Cut 1995: (a) Ri_x (solid line) computed from observed tidal currents and dS/dx—the critical value of $Ri_x = 0.6$ is also shown (dashed line); (b) strength of gravitational circulation PC_2 (cm s^{-1}); (c) near-bottom salt flux (+ upstream), decomposed as total salt flux (solid line), salt flux due to tidal averages $\langle U\rangle\ \langle S\rangle$ (dot–dash line), and salt flux due to tidally fluctuating salinities and velocity $\langle U'S'\rangle$ (dashed line), where U' and S' are the instantaneous deviations from the low-pass filtered values $\langle U\rangle$ and $\langle S\rangle$

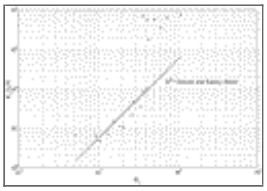

Click on thumbnail for full-sized image.

FIG. 16. The dependence of $K_x/(u_* H)$ on Ri_x as computed using a one-dimensional water column model that includes tidally varying stratification

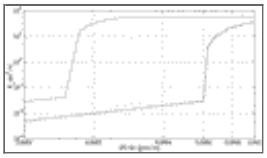

Click on thumbnail for full-sized image.

FIG. 17. Plot of K_x as a function of dS/dx averaged over two spring–neap cycles: solid line is 10 m and dashed line is 20 m. The instantaneous values of K_x used are those given in Fig. 16

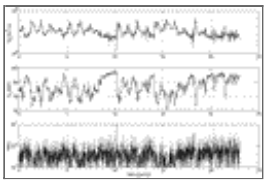

Click on thumbnail for full-sized image.

FIG. A1. Plot of (a) Q_f(m^3 s^{-1}), (b) X_2(km), and (c) ratio of $\partial S/\partial t$:$u\partial S/\partial x$. The dots represent the raw daily data and the lines represent the raw data low-pass filtered with a fourth-order Butterworth filter with a 14-day time constant

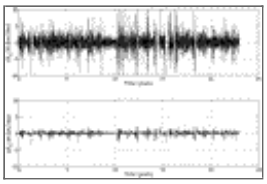

Click on thumbnail for full-sized image.

FIG A2. Time series of (a) raw dX_2/dt and (b) low-pass filtered dX_2/dt

Corresponding author address: Dr. Stephen Monismith, Department of Civil and Environmental Engineering, Environmental Fluid Mechanics and Hydrology, Stanford University, Terman Engineering Center, Stanford, CA 94305-4020. E-mail: monismith@ce.stanford.edu

[1] A description of the method can be found online at http://iep.water.ca.gov/dayflow/.

[2] Data are available online at http://sfbay.wr.usgs.gov/access/wqdata/index.html.

[3] Salinity data from USGS stations were provided by R. Oltmann of the USGS California district.

[4] The potential effects of unsteadiness on the steady salt balance used in this paper are discussed in the appendix.

top